



APPLICATION OF THE ADAPTIVE ARRAY REDUCTION METHOD USING LOGARITHMIC SPIRAL INITIAL STENCILS

Elias Arcondoulis and Yu Liu

Department of Mechanics and Aerospace Engineering, Southern University of Science and Technology
1088 Xueyuan Blvd, Nanshan, 518055, Shenzhen, P.R. China

Abstract

The Adaptive Array Reduction Method (AARM) was recently developed as an alternative to conventional array designs, such as logarithmic spirals and multi-arm spiral array designs. In the AARM, the number of channels in an initial array is reduced numerically, by removing microphones that provide the least contribution to the array's Point Spread Function (PSF) maximum sidelobe level and main lobe width. To date the AARM has only been applied to grid-based stencils, such that the initial array possesses some grating lobes near the main lobe perimeter. This paper presents the results of using the AARM with logarithmic spiral arrays as the initial stencil. This effectively takes advantage of the best qualities of both methods: the initial array logarithmic spiral PSF is typically clear of strong sidelobes and always clear of grating lobes and the AARM seeks to reduce the array while compromising the PSF as little as possible. It is revealed that by using 48-channel arrays that are designed for a single frequency over a logarithmic spiral stencil, comparable performance to a 200-channel logarithmic spiral array can be achieved. This can be practically implemented using a multiplexer hardware configuration.

1 INTRODUCTION

For most acoustic beamforming method and applications [1, 2], logarithmic spiral arrays provide a well-suited balance between Maximum Sidelobe Level (MSL) and Main Lobe Width (MLW) for varying source locations across a scanning grid and a range of acoustic frequencies [3–5] that can be adapted for a range of applications and challenging environments [6–9]. A recently published array design method, namely the Adaptive Array Reduction Method (AARM) [10] has been successfully shown to act as an alternative to logarithmic spiral array designs. The AARM arrays can be easily customised for specific beamforming frequencies, frequency range,

anticipated source locations and can be designed over any area. The AARM design uses an iterative microphone removal process, to determine the best case array possible based on the initial array stencil from which it is removed, based predominantly on MSL and MLW criteria. To date, only grid-based initial stencils have been investigated [10, 11]. In this paper, the AARM will be applied to a 200-channel logarithmic spiral array design, over a range of frequencies and two source locations. By using a logarithmic spiral initial array, the Point Spread Function (PSF) of the reduced array during the early stages of array reduction should be of excellent quality [4, 5, 8]. When the AARM is used over a grid based stencil, the early iteration stages focus on removing the grating lobes near the main lobe perimeter, which is common for grid-based array designs [12]. By using a logarithmic spiral initial array, this can be avoided as its PSF will not contain any grating lobes and at worst, only weak sidelobes will appear predominately near the scanning grid outer regions [4, 5].

The motivation for conducting such a study is for testing facilities that are limited to a relatively small number of Data Acquisition (DAQ) channels [7, 8] and require versatility to maximise the total capability of their microphone and DAQ system. In this paper, it is revealed that by using a series of 48-channel single frequency arrays designed using the AARM that comparable performance can be achieved to a 200-channel logarithmic spiral array, in terms of MSL and MLW. While at each beamforming frequency a separate array design is required, which at first seems extremely impractical, by the use of multiplexer (MUX) hardware many array designs can be tested experimentally without needing to manually change the array pattern, provided that the initial stencil is fully populated with microphones. By taking advantage of the AARM's ability to easily and quickly produce array designs for specific frequencies and locations, and how much cheaper a microphone is relative to a DAQ channel, high channel count beamforming array design can be obtained using far fewer DAQ channels, thus saving costs and time.

2 METHODOLOGY

The methodology of this paper is to apply the AARM using logarithmic initial stencils. Therefore to explain the methodology, the AARM processes, including the cross-spectral beamforming method, and the equations used to generate logarithmic spirals are summarised here.

2.1 Cross-Spectral Beamforming

A spherical wave source (i.e., a monopole source) of unit source strength in still conditions is simulated. The propagation of this wave to the array plane can be represented as \mathbf{p} , a vector of complex pressures (Pa) in the frequency domain ($M \times 1$ vector), defined as

$$\mathbf{p} = \frac{1}{4\pi|\mathbf{r}_s|} \exp\left[\frac{-j2\pi f\mathbf{r}_s}{c_0}\right] \quad (1)$$

where f represents both the source frequency and the array design frequency (Hz), c_0 is the speed of sound in air (343 m/s) and m denotes the microphone number ranging from 1 to M , where M is the number of microphones in the array at each step of the AARM. The vector \mathbf{r}_s links the simulated source location to each of the microphone coordinates in the array plane.

The complex pressures at each microphone generated in Eq. (1) are used to produce a Cross-Spectral Matrix, C [13] (also referred to as CSM), which is an $M \times M$ matrix defined as

$$C = \mathbf{p}\mathbf{p}^H \quad (2)$$

where H represents the complex transpose and conjugate. The diagonal entries are set to zero to remove the autospectra from the matrix [13]. A beamforming output is computed over a planar discretised grid of N data points (scanning grid) at a known distance from the array, typically positioned in line with the centre of the microphone array. Steering vectors, \mathbf{v} , contain the unique distances of each scanning grid point to each microphone, m . The steering vector formulation for the m^{th} microphone used here [14] is an $N \times 1$ array defined as

$$\hat{\mathbf{v}} = \frac{1}{4\pi|\mathbf{r}_m|} \exp\left[\frac{-j2\pi f\mathbf{r}_m}{c_0}\right] \quad (3)$$

where \mathbf{r}_m is the vector between the scanning grid point to the microphone m . The cross-spectral beamforming output, Y (Pa^2), [14] is computed using

$$Y(\hat{\mathbf{v}}) = \frac{\hat{\mathbf{v}}^H \{\mathbf{w}C\mathbf{w}^H\} \hat{\mathbf{v}}}{(\sum_{m=1}^M \mathbf{w})^2 - (\sum_{m=1}^M \mathbf{w})} \quad (4)$$

where \mathbf{w} represents the $1 \times M$ microphone shading vector. The shading quantity adjusts the microphone pressures relative to each other. In the AARM to produce the array design, the entries of \mathbf{w} (i.e., $w(m)$) are either 0 or 1 to simulate a microphone being removed or included in the array respectively. Once the array is created, the entries of \mathbf{w} are equal to 1 to produce the PSF and to conduct other beamforming simulations.

At each frequency, f , the MLW is calculated first by determining how many scanning grid points the main lobe covers until it decreases by 3 dB from the main lobe peak. This -3 dB definition is consistent with others [14–16] yet the evaluation of an MLW value is unique and is based on a square-rooted area ratio of the -3 dB main lobe area and the number of scanning grid points, similar to previous array reduction publications [10, 11].

A larger region calculated around the main lobe named the Main Lobe Area (MLA) is defined here by 30 dB below the normalised main lobe peak. Due to the potential asymmetry of the main lobe, the bounds of the MLA are calculated in both the x - and y -directions, namely $\text{MLA}(x)$ and $\text{MLA}(y)$ respectively. The MLA is removed from the image source map so that the remaining source map does not contain the main lobe to within 30 dB of the main lobe peak. The MSL can then be calculated using the maximum remaining Y value, Y_s . The MSL and MLW in this paper are represented as

$$\text{MSL}(\text{dB}) = 10 \log_{10} \left\{ \frac{Y_s}{Y_{\max}} \right\} \quad (5)$$

$$\text{MLW}(\%) = 100 \times \sqrt{\frac{N_{3\text{dB}}}{N}} \quad (6)$$

where Y_{\max} is power of the the non-normalised main lobe pressure (Pa^2) and $N_{3\text{dB}}$ is the number of scanning grid points that are occupied by the main lobe from its normalised maximum amplitude (0 dB) to -3 dB.

2.2 Adaptive Array Reduction Method

The AARM is an advancement of the ARM [11], where the dimensionless metric, Φ , is defined simply as the product of the MSL and MLW

$$\Phi = 10 \log_{10} \left\{ \frac{Y_s}{Y_{\max}} \times \frac{N_{3\text{dB}}}{N} \right\} + 20 \quad (7)$$

In the AARM [10] the evaluation of Φ is dependent upon a coefficients a and L_D , defined as $\Phi_{a,l}$

$$\min \{ \Phi_{a,l} \} \equiv \min \left\{ \left[\frac{Y_s}{Y_{\max}} \right]^a \times [N_{3\text{dB}}]^{1-a} \times L_D \right\} \quad (8)$$

where a is a value between 0 and 1 that is calculated based on previous reduction steps of the AARM to give greater emphasis on minimising either the MSL or MLW. The term L_D is a lobe-distortion term that measures the size of the MLW in every 45° direction, and then takes the ratio of the greatest and smallest values to determine how distorted MLW is (i.e., a purely circular main lobe has $L_D = 1$, such that no lobe-distortion penalty is applied, and an elliptical main lobe with orthogonal axes that have length x and $y = 2x$ will have $L_D = 2$). Now that $\Phi_{a,l}$ has been introduced, the AARM algorithm is explained as follows:

1. An initial array stencil is used that is composed of a larger number of microphones, M_i , relative to the desired number of microphones, M_f . Every microphone from $m = 1:M_i$ is shaded one-at-a-time using w .
2. Let m' be the microphone that is shaded, so that $w(m') = 0$ and $w(m) = 1$, for $m = 1:M_i$ where $m \neq m'$. The beamformer output Y is calculated for every m' value of m in $1:M_i$. The microphone number m' that produces $\min \{ \Phi_{a,l} \}$ will be removed from the array (i.e., removing this microphone causes the smallest negative impact on Y).
3. The size of the array then decreases by one and the next shading process commences: $w(m') = 0$ and $w(m) = 1$, for $m = 1:M_i - 1$ where $m \neq m'$.
4. This process is repeated until the predetermined desired number of microphones remains within the array stencil, M_f .

The variation of a throughout the simulation is determined by the change of MSL and MLW as the simulation progresses (i.e., their local derivatives with respect to m). The local derivatives of MSL and MLW are calculated using a five-point-centred finite difference scheme. Details of this procedure and the values of a per iteration can be sought in Arcondoulis and Liu [10].

2.3 Logarithmic Spiral Initial Stencil Design

Logarithmic spirals are investigated here as a type of initial stencil for the AARM because they possess the highest number of unique spacing between microphones as compared to other array types of the same size and number of microphones [5]. The parametric equations that represent the logarithmic spiral coordinates (x and y) can be written as

$$x(m) = \alpha \cos[\theta(m)] e^{\beta\theta(m)} \quad (9)$$

$$y(m) = \alpha \sin[\theta(m)] e^{\beta\theta(m)} \quad (10)$$

where α and β are coefficients that affect the overall size of the spiral and how rapidly the arms of the spiral expand from the centre respectively. The angle $\theta(m)$ is defined as

$$\theta(m) = \frac{2\pi(m-1)l}{M} \quad (11)$$

where l influences the number of spiral revolutions of the array pattern. An $M_i = 200$ -channel logarithmic spiral initial stencil is designed using the parameters $\alpha = 80$, $\beta = 9$, $l = 38$, $M = 200$ and is presented in Fig. 1. This stencil can also be observed as grey-dots in Figs. 4 and 5. The spiral array possesses many microphones near the centre of the array area and gradually decreases in microphone density with increasing distance from the centre. Microphones near the outer limits of the spiral arms ensure that the array aperture is sufficient to perform well at 2 kHz (which is the lower frequency bounds adopted in Section 2.4) yet there is a dense tightly-spaced cluster of microphones near the centre to ensure good performance at 8 kHz, corresponding to the prescribed upper frequency bound. The initial stencil array spans approximately $0.6 \text{ m} \times 0.6 \text{ m}$.

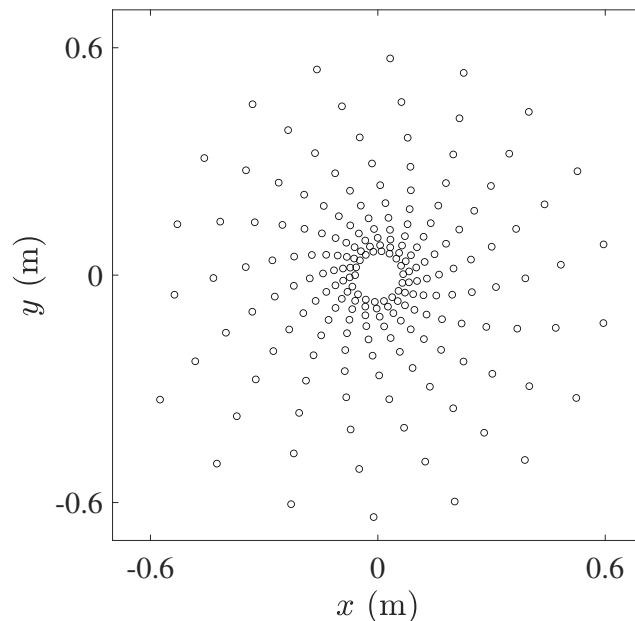


Figure 1: The $M = 200$ initial stencil used for the AARM simulations. This logarithmic spiral array pattern was generated using Eqs. (9) to (11) and parameters $\alpha = 80$, $\beta = 9$, $l = 38$ and $M = 200$.

2.4 Simulation Conditions

To conduct the AARM, a series of parameters must be considered, such as the final array channel count. Each array considered here is reduced from $M_i = 200$ -channels to $M_f = 48$ -channels. A minimum, maximum and frequency increment must be defined, based on the desired beamforming frequency range. AARM arrays can be produced over a frequency range or at a single frequency. The arrays designed over a frequency range are created by taking the frequency-averaged MSL and frequency-averaged MLW and using these parameters in Eq. (8) to determine which microphones should be iteratively removed [10, 11]. The frequencies considered for the AARM in this paper are $f_{\min} = 2$ kHz and $f_{\max} = 8$ kHz. Both single frequency arrays ($f_s = 1$) and multiple-frequency arrays ($f_s > 1$) are presented, both using the same f_{\min} and f_{\max} . The multiple-frequency array uses $f_s = 13$ (such that each investigated frequency was equispaced by 0.5 kHz), as is simply referred to as the $f_s = 13$ array. The single frequency arrays are generated between f_{\min} and f_{\max} and are denoted as $f_s = 1$ (2 kHz), to denote a single-frequency array generated for a 2 kHz source, for example.

Another important input of the AARM is the location of the source on the scanning grid, to produce a PSF possessing unique MSL and MLW values. This source can be located theoretically anywhere on the scanning grid location, yet the quality of the array is likely to be biased to this simulated source location. Thus, and in accordance with other beamforming array design methods [8, 11, 12, 15, 17], arrays are generated using a simulated source located at the centre of the scanning grid, being $x = y = 0$ m, hereby denoted as centred arrays. To further test the AARM using a logarithmic array initial stencil, arrays are also designed using an off-centred source, located at $x = 0.1$ m and $y = 0.2$ m from the centre of the scanning grid, hereby denoted as off-centred arrays.

For the AARM simulations presented, the scanning grid consists of $51 \times 51 = N = 2,601$ scanning grid points, spanning an area of $1 \text{ m} \times 1 \text{ m}$ located $z = 1$ m from the array plane. To accurately determine quantities such as MSL and MLW using the $M_f = 48$ -channel arrays, a finer scanning grid of $101 \times 101 = N = 10,201$ scanning grid points is used. Such a refined scanning grid would be time prohibitive for the AARM simulations and previous publications have shown that high quality arrays can be produced using an $N = 2,601$ scanning grid [10, 11].

It should be noted that if scanning grid area is much larger during the AARM, then a greater proportion of sidelobes will appear near the perimeter of the scanning grid, thus heavily influencing the AARM method, as it attempts to minimise the growth of MSL during the reduction process. Furthermore, by increasing the scanning grid area, the MLW covers fewer scanning grid points (as compared to the same number of grid points covering a smaller area) and therefore will make lobe distortion estimations less accurate (due to the fewer number of scanning grid points covered by the MLW)

3 RESULTS

The results are presented in a form of chronological order. Firstly, the array reduction process reveals the performance of the AARM arrays from M_i to M_f channels and how the MSL and MLW evolves during the AARM process. Secondly, the generated arrays are presented with the initial stencil and their PSF maps are presented for some of the investigated frequencies. Further performance analysis of each array design is conducted, by presenting the MSL and MLW values with respect to beamforming frequency to reveal a frequency-dependent comparison of the arrays. Lastly, a multi-array concept using the AARM is presented, that utilises a multiplexer (MUX) that uses several arrays during simultaneous experiment that exploits the benefits of using several $f_s = 1$ arrays at each frequency as compared to a single $f_s = 13$ array.

3.1 Array Reduction Process

To determine the effectiveness of the AARM to produce an M_f -array from M_i -channels, the evolution of the array performance for the $f_s = 13$ arrays are analysed.

Firstly, the centred array is considered. Figure 2 presents the evolution of the frequency-averaged MSL and MLW with increasing number of microphones removed for the centred $f_s = 13$ array. The data are normalised to initial stencil frequency-averaged MSL and MLW values to help visually compare the changes of MSL and MLW values simultaneously. For the first

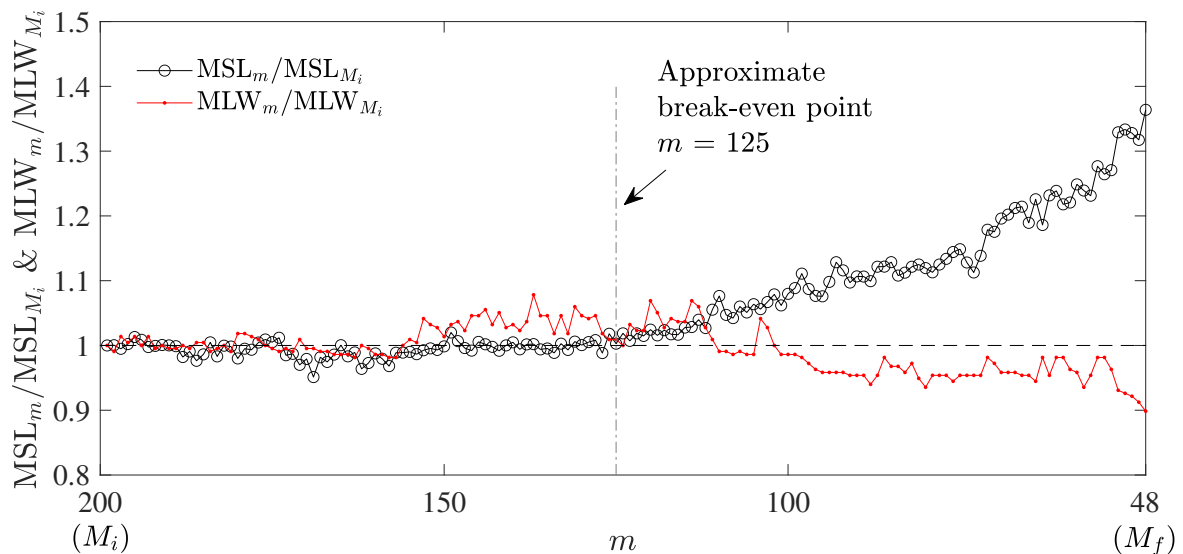


Figure 2: The evolution of the frequency-averaged MSL_m and MLW_m with respect to microphone number, m , for the AARM using a source located at $x = y = 0$. The data are normalised relative to the initial stencil frequency-averaged MSL and MLW values, being MSL_m / MSL_{M_i} and MLW_m / MLW_{M_i} , respectively. A vertical line is drawn at $m = 125$ to represent a break-even point where both quantities are approximately equal to one, and a horizontal line is drawn at a value of one to help identify values above and below unity.

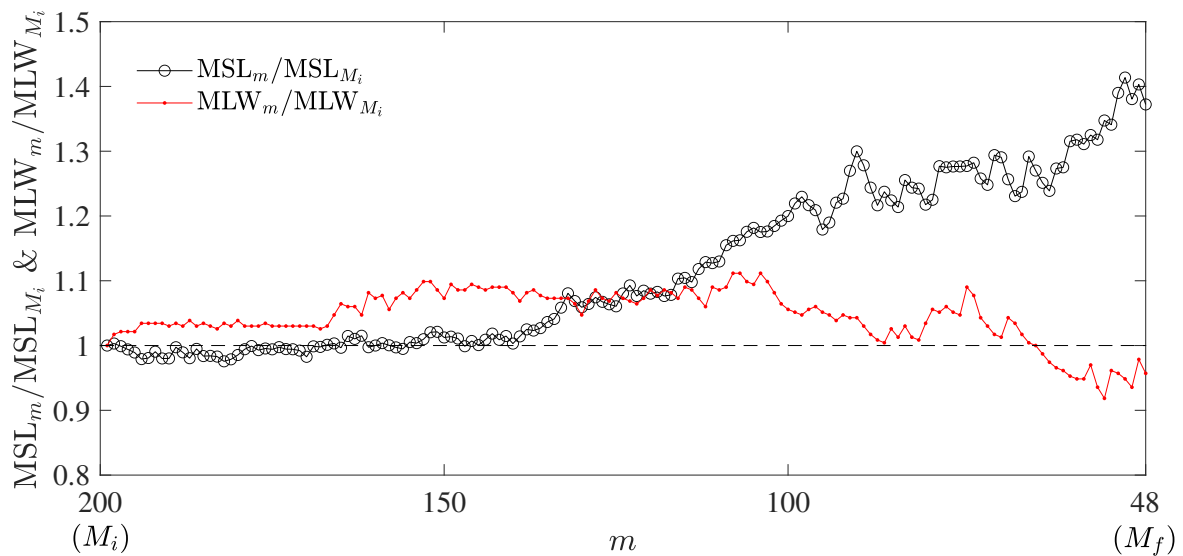


Figure 3: The evolution of the frequency-averaged MSL_m and MLW_m with respect to microphone number, m , for the AARM using a source located at $x = 0.1$ m and $y = 0.2$ m. The data are normalised relative to the initial stencil frequency-averaged MSL and MLW values, being MSL_m/MSL_{M_i} and MLW_m/MLW_{M_i} , respectively. A horizontal line is drawn at a value of one to help identify values above and below unity.

forty microphones removed (from $M_i = 200$ to $m = 160$) it can be seen that there is little change in MSL and MLW. The break-even point at $m = 125$ reveals that seventy-five microphones can be removed from the initial array of $M_i = 200$ microphones to produce an AARM array that possesses the same frequency-averaged MSL and MLW values over the frequency range of $f = 2$ kHz to 8 kHz for a source located at the centre of the scanning grid. With further microphone removal (i.e., increasing m), the MSL values steadily increase, which is expected with an array of fewer microphones [5, 8, 12]. The final MSL value is 1.36 times greater than the value of the $M_i = 200$ -channel array, as observed on the right-hand side y -axis. The MLW, however, interestingly decreases and continues to do so for the entire reduction process to $M_f = 48$ (on average, after the break-even point) to 0.90 times the value of the $M_i = 200$ -channel array.

The evolution of MSL and MLW during the AARM for the off-centred $f_s = 13$ array is presented in Fig. 3. It can be seen that there is no break-even point for this specific off-centred array condition ($x = 0.1$ m and $y = 0.2$ m) as observed for the centred array design process, shown in Fig. 2. However, the $M_f = 48$ array has a similar relative MSL value as the centred array, being 1.38, and a similar MLW value of 0.97, revealing that the AARM process has performed similarly overall for both the centred and off-centred array designs.

3.2 Array Patterns

The centred array patterns generated using the AARM are presented in Fig. 4. The array produced by the $f_s = 13$ simulation, analysed and discussed in Section 3.1, is firstly discussed. It can be observed that not all of the initial stencil spiral arms are populated and similarly the centre cluster region is also not fully populated, as the AARM attempted to provide a balance between low and high frequency beamforming conditions. The single-frequency arrays, denoted by $f_s = 1$ and their corresponding frequency in Fig. 4, each reveal unique frequency-dependent microphone arrangements. With increasing frequency from 2 kHz to 8 kHz it can be observed that the microphones shift toward the centre. At 2 kHz to 4 kHz there are several microphones near the array outer perimeter to improve the MLW, yet at 5 kHz and greater all of the microphones are located much closer to the geometric centre of the stencil. As the frequency increases, the density of microphones near the geometric centre increases to improve the MSL. These array properties are also observed when the AARM is applied over a grid-based stencil [10], in terms of the distribution of microphones relative to the array centre.

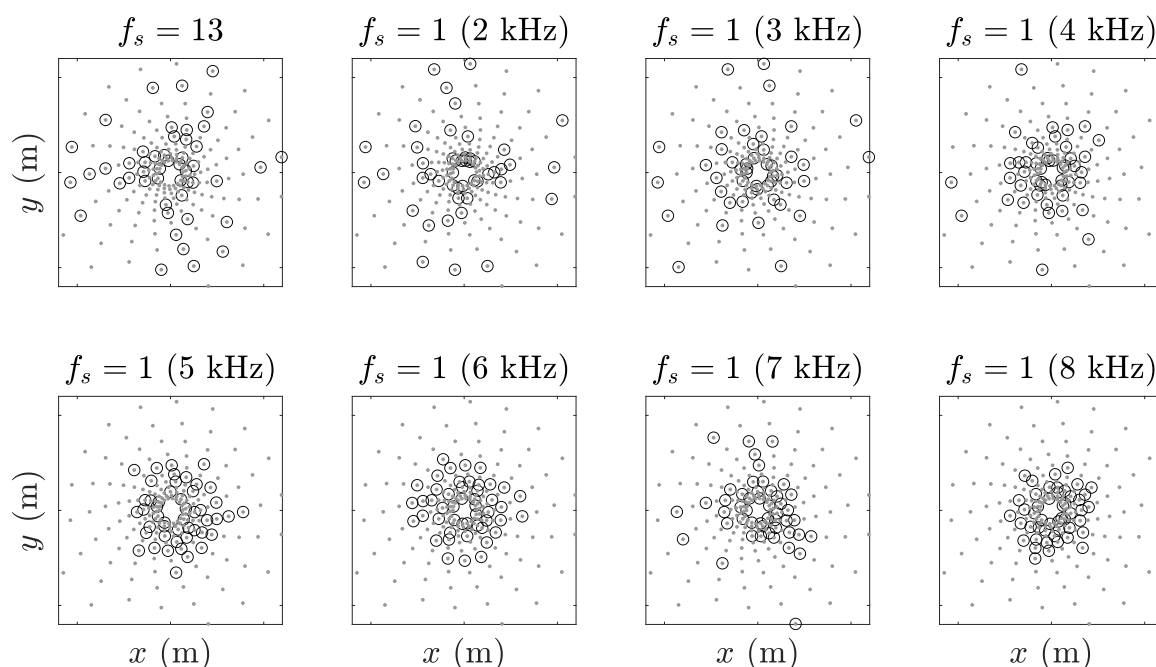


Figure 4: Centred arrays: The initial logarithmic spiral $M = 200$ -channel array (represented by grey dots) and the reduced AARM 48-channel array (represented by open circles). Arrays are designed using the AARM with a source located at $x = y = 0$ m and $z = 1$ m for $f = 2$ kHz to 8 kHz. Each array is bounded by a 0.6 m \times 0.6 m area.

The off-centred array designs are presented in Fig. 5. Recall that these arrays are designed based on a simulated source located at $x = 0.1$ m and $y = 0.2$ m. The $f_s = 13$ array pattern differs from the centred equivalent, as there is a greater cluster of microphones near the centre. There are also several microphones near the array outer perimeter to ensure MLW performance at lower frequencies. A similar array pattern is observed for the single-frequency off-centred array

at 2 kHz. At frequencies 3 kHz and greater, it can be seen that the majority of the microphones are positioned in the upper-right quadrant of the array area, corresponding to the approximate source location. This is expected, as the greater the population of microphones centred about the source location, the better the MSL and MLW performance. As the frequency increases, unlike the centred-array designs, the microphones remain distributed over a larger area. This was done by the AARM to ensure that the MLW is not enlarged and the lobe-distortion remains as low as possible. Nonetheless, the microphone density near the geometric centre increases with increasing frequency.

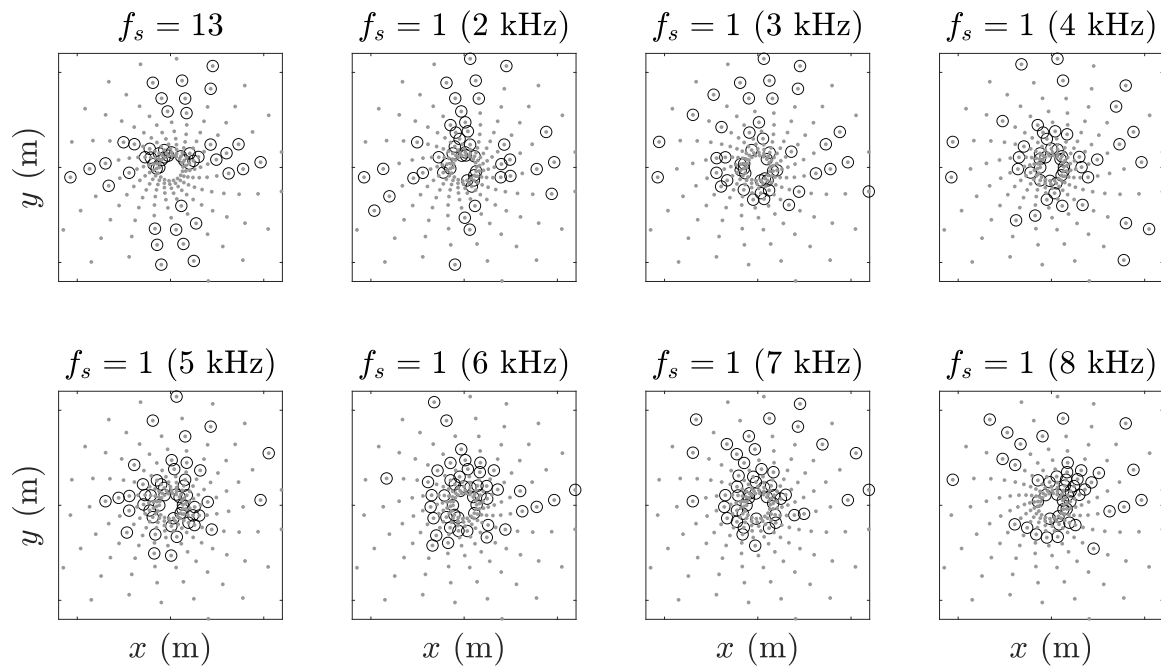


Figure 5: Non-Centred arrays: The initial logarithmic spiral $M = 200$ -channel array (represented by grey dots) and the reduced AARM 48-channel array (represented by open circles). Arrays are designed using the AARM with a source located at $x = 0.1$ m, $y = 0.2$ m and $z = 1$ m for $f = 2$ kHz to 8 kHz. Each array is bounded by a 0.6 m \times 0.6 m area.

3.3 Array Performance

The beamformer outputs (Y , corresponding to the PSFs) using both the initial and reduced centred arrays are presented in Fig. 6. Each array is tested at $f = 2$ kHz, 5 kHz and 8 kHz, as identified on the right-hand side of the figure. The $f_s = 1$ PSFs are generated using their appropriate $f_s = 1$ array (e.g., the $f_s = 1$ (2 kHz) array in Fig. 4 is used to produce the $f_s = 1$ PSF at 2 kHz for the centred array condition).

For the initial stencil (i.e., $M = 200$ -channel array), it can be observed that each map shows a symmetric main lobe without noticeable distortion and no visible sidelobes within -20 dB of

the main lobe peak. This is a typical result for a high-quality logarithmic spiral array, tested by a simulated source at the scanning grid centre. The $f_s = 13$ array shows some smearing of the main lobe at approximately -10 dB and lower from the main lobe peak. This is consistent for each of the frequencies presented. At 5 kHz and 8 kHz, there are several sidelobes scattered about the scanning grid, all of which are less than -10 dB. Clearly the performance of the 48-channel $f_s = 13$ array here is not a suitable array design and has a much poorer performance than the $M = 200$ -channel array.

By utilising the AARM's ability to produce an array with good MSL and MLW properties at a single frequency (at the expense of performance at other frequencies [11]), the performance of the $f_s = 1$ arrays on average shows better MSL and MLW performance relative to the $f_s = 13$ array. The results at 2 kHz are similar between the $f_s = 1$ and $f_s = 13$ array, yet at 5 kHz and 8 kHz, there are significant differences in the PSFs. It appears that the $f_s = 1$ arrays have MSL

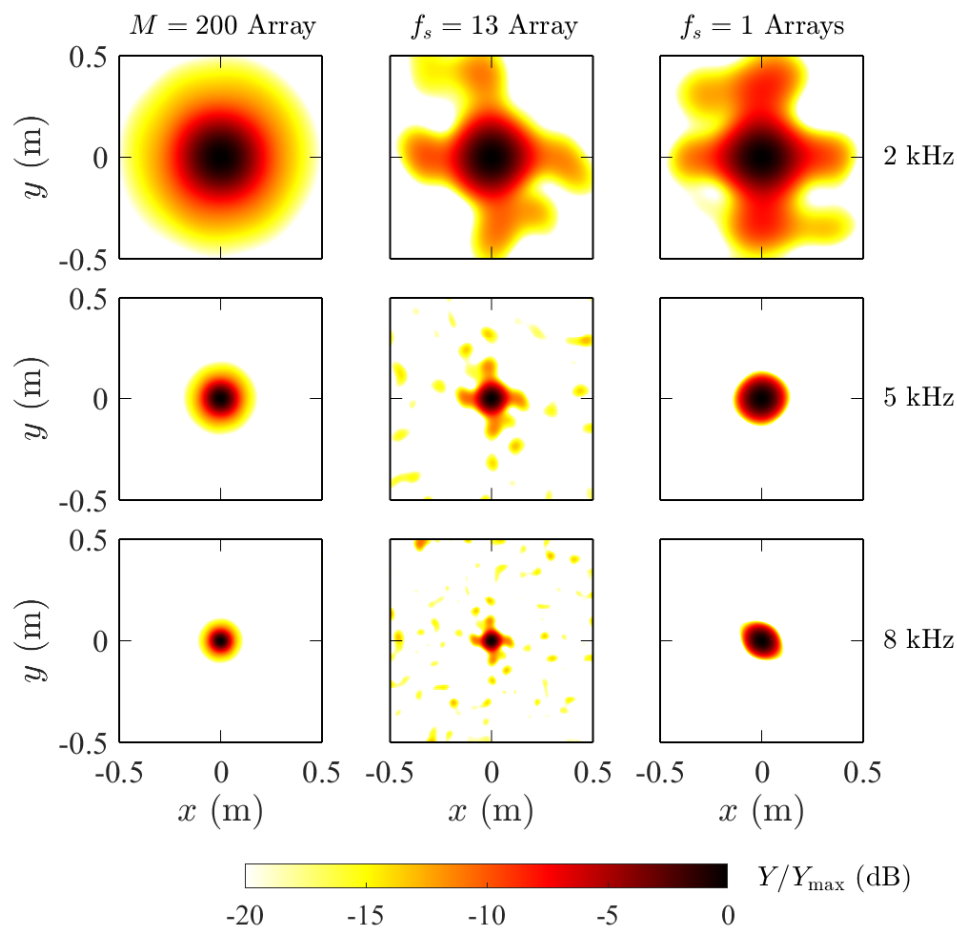


Figure 6: Comparison of the initial logarithmic spiral $M = 200$ -channel array and AARM 48-channel $f_s = 13$ array and applicable $f_s = 1$ array PSFs for a single-source located at $x = y = 0$ m and $z = 1$ m for frequencies $f = 2$ kHz, 5 kHz and 8 kHz. The dB scale is Y normalised to the main lobe magnitude Y_{\max} .

values below -20 dB like the $M = 200$ -channel array yet have greater MLW values. Note that the MLA for each array is quite similar, yet the MLW (defined as the -3 dB region of the main lobe) is greater for the $f_s = 1$ arrays and at 8 kHz, the $f_s = 1$ array possesses some lobe distortion.

The performance of the AARM off-centred arrays is typically poorer than the centred arrays, especially for the $f_s = 13$ array, as can be observed by comparing the centred array performance in Fig. 6 with the off-centred array performance in Fig. 7. The $M = 200$ -channel array performs well with an offset source, as expected with a well-designed spiral array possessing many channels. The main lobes are quite symmetric, and the only appearance of weak sidelobes occurs at 8 kHz, near the scanning grid perimeter. The AARM method, using a logarithmic spiral however, has not performed well for the $f_s = 13$ condition. There appear to be secondary lobes that are mirrored from the main lobe about the horizontal axis. In addition, at each frequency, there are

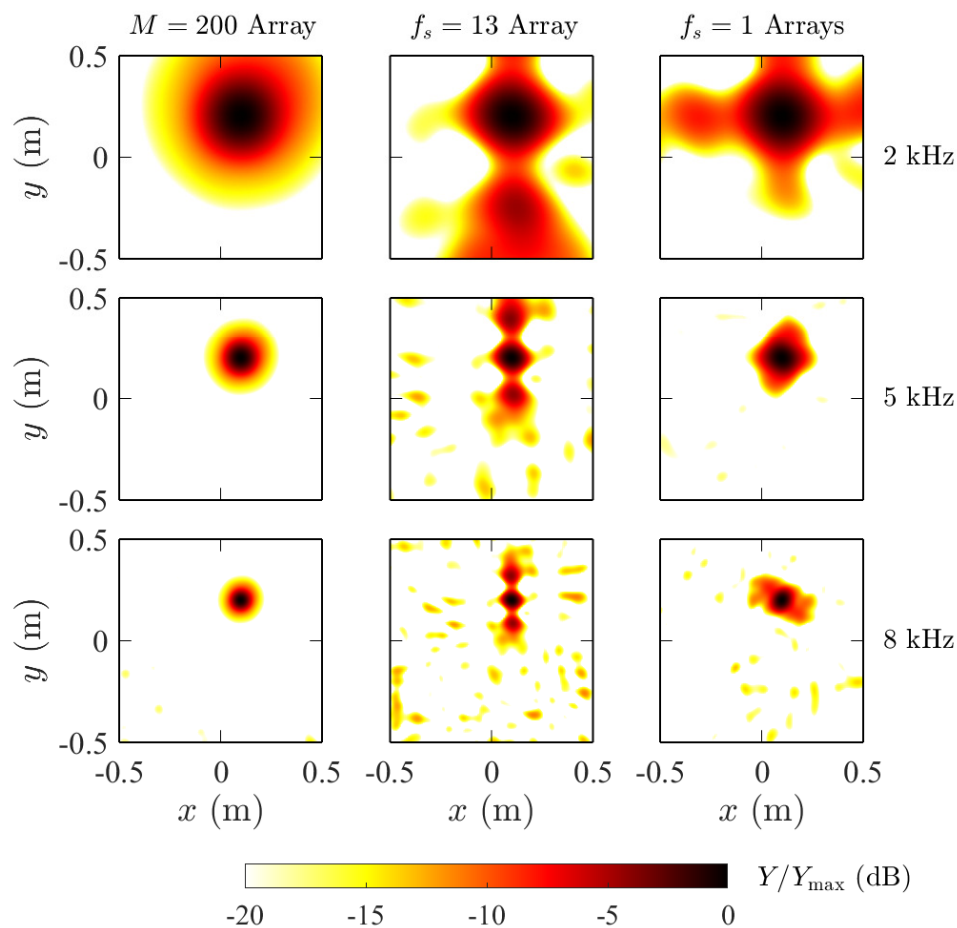


Figure 7: Comparison of the initial logarithmic spiral $M = 200$ -channel array and AARM 48-channel $f_s = 13$ array and applicable $f_s = 1$ array PSFs for a single-source located at $x = 0.1$ m, $y = 0.2$ m and $z = 1$ m for frequencies $f = 2$ kHz, 5 kHz and 8 kHz. The dB scale is Y normalised to the main lobe magnitude Y_{\max} .

sidelobes scattered about the scanning grid area. By using specific $f_s = 1$ arrays however, the PSF at each frequency is much improved. The main lobes, despite some smearing between -5 dB and -10 dB of the main lobe peak, have comparable MLW values to the $M = 200$ -channel array. At 2 kHz and 5 kHz, only very weak sidelobes can be observed. At 8 kHz, the sidelobes are slightly stronger yet their magnitude is relatively small, being approximately -15 dB.

To evaluate the performance of each array over a range of frequencies, the MSL and MLW values are calculated between $f_{\min} = 2$ kHz and $f_{\max} = 8$ kHz, to coincide with the design frequencies of the AARM arrays. The results for the centred-arrays are presented in Fig. 8. For each frequency, the $M = 200$ -channel array outperforms the $f_s = 13$ -array for every frequency in terms of MSL, as expected. Both arrays show a slight increase of MSL with respect to frequency, which is again as expected for a well-designed array. The $f_s = 1$ -arrays show slightly lower MSL values (on average) relative to the $M = 200$ -channel array. An exception occurs at $f = 7$ kHz, where the MSL appears is greater. Nonetheless, these results show that by using a specific $f_s = 1$ -array with 48-channels, comparable if not improved MSL performance relative to a well-designed 200-channel array can be achieved. The MLW values of the $M = 200$ -

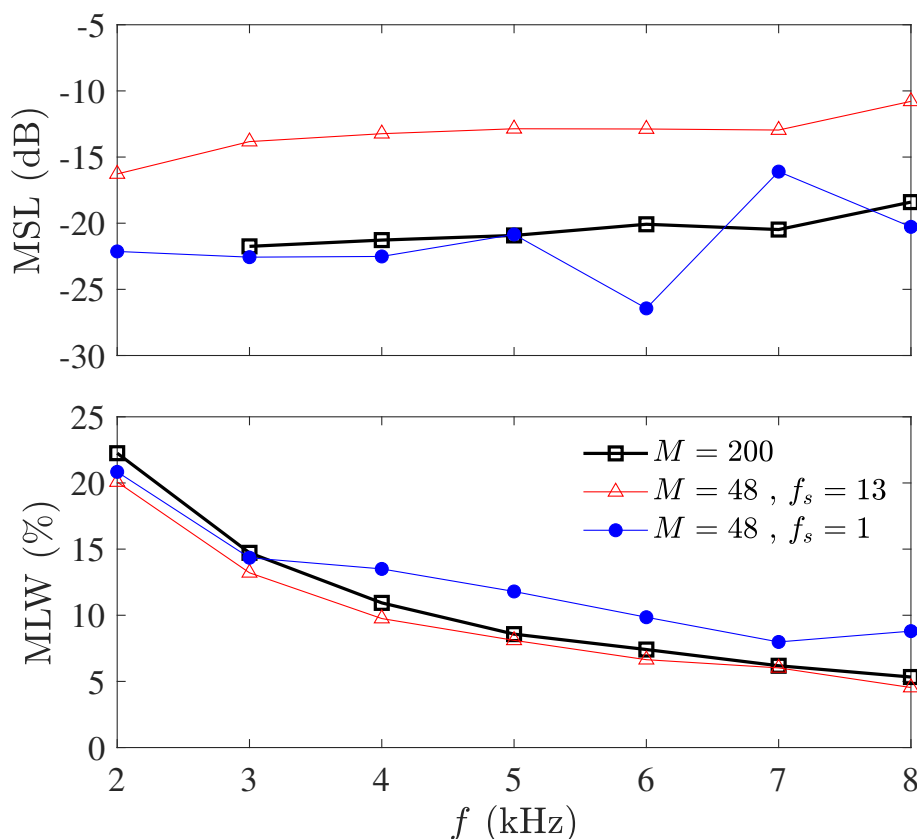


Figure 8: The performance of the centred arrays in terms of MSL and MLW with respect to PSF frequency, for a source located at $x = y = 0$ m and $z = 1$ m. The $M = 200$ -array and $f_s = 13$ -array data are obtained from a single array and the $f_s = 1$ -arrays are obtained from their specific array for that frequency.

channel array and the $f_s = 13$ -array are quite similar, and at some frequencies the $f_s = 13$ -array possesses lower MLW values. While this is an attractive property, it cannot be seen as an overwhelming positive as the main lobe area at magnitudes less than -3 dB from the main lobe peak showed some smearing and distortion (as presented in Fig. 6). While the $f_s = 1$ -arrays showed comparable MSL values to the $M = 200$ -channel array, their MLW values are typically greater, with exceptions at $f = 2$ kHz and 3 kHz. Overall, from the source maps presented in Fig. 6 and the MSL and MLW values shown in Fig. 8, the 48-channel $f_s = 1$ -arrays show reasonable performance relative to the $M = 200$ -channel array, considering the significant difference in total number of channels used.

The MSL and MLW values for the off-centred arrays are presented in Fig. 9. By comparison between the centred and off-centred array results, it can be seen that the difference in MSL values of the $f_s = 1$ -arrays and the $M = 200$ -array is greater for the off-centred arrays. Other than at $f = 2$ kHz and 3 kHz, the $f_s = 1$ -array MSL is on average approximately 3 dB greater than the $M = 200$ -array. Each array's MSL values approach each other at higher frequencies, especially at 8 kHz, where the difference in MSL between each array is less than 5 dB. The

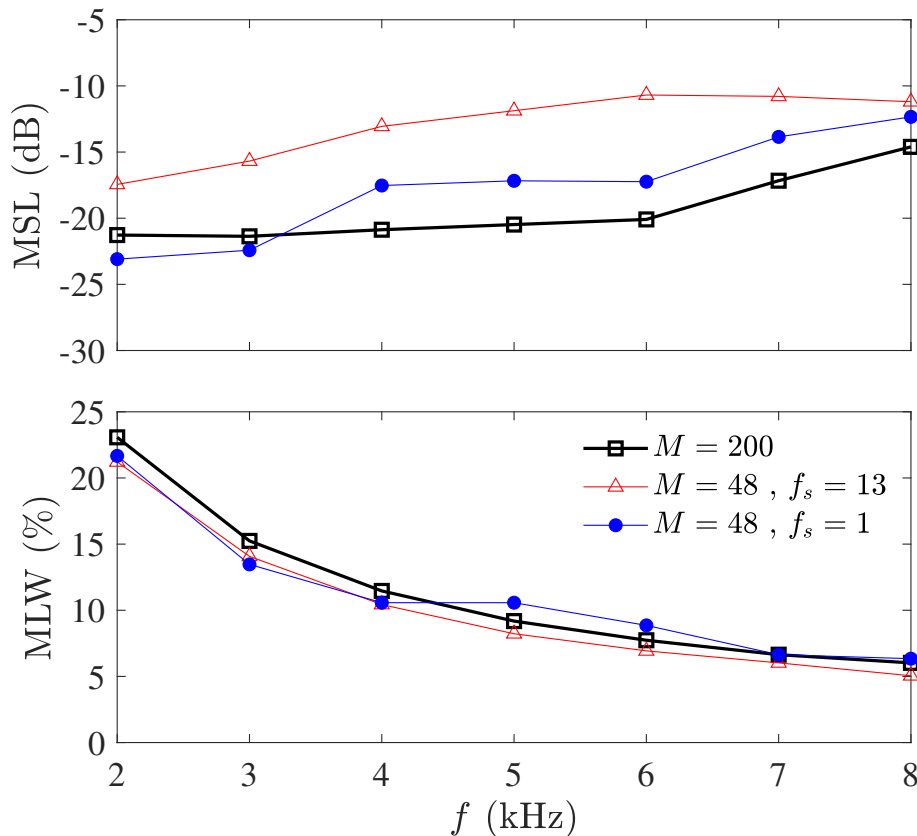


Figure 9: The performance of the off-centred arrays in terms of MSL and MLW with respect to PSF frequency, for a source located at $x = 0.1$ m, $y = 0.2$ m and $z = 1$ m. The $M = 200$ -array and $f_s = 13$ -array data are obtained from a single array and the $f_s = 1$ -arrays are obtained from their specific array for that frequency.

MLW values for each off-centred array are much closer than the centred arrays. The MLW values of the $f_s = 1$ -arrays are quite comparable to the $M = 200$ -array, with two exceptions at $f = 5$ kHz and 6 kHz. From these results, it can be seen that the off-centred $f_s = 1$ -arrays perform well, relative to the $M = 200$ -array, where both the MSL and MLW values are comparable.

3.4 Multiplexer Concept

From the arrays presented in this paper, the $f_s = 1$ -array single-frequency performance seems attractive, as these arrays possess far fewer microphones than the initial stencil that they were derived from. The arrays are simple to design using the AARM method and they fit within a predefined stencil that does not need to change. However, the idea of using $f_s = 1$ -arrays may seem impractical, in that a new array would need to be installed during an experiment for every frequency of interest. Replacing microphones within an array stencil for many different AARM array configurations during experiments is possible yet could be quite tedious if the number of different array patterns is large. Alternatively, the cost of a 200-channel DAQ system (or a system with a number of channels to the nearest multiple of 8 or 16, as typically used in DAQ hardware) far exceeds that of a 48-channel DAQ system.

A practical solution is discussed here that makes use of two major factors: (1) the cost of microphones are typically far less than the cost of a DAQ channel. Acoustic beamforming can be successfully conducted using cheap microphones, provided that they are calibrated individually and the array PSF is also calibrated [7], and (2) the AARM is a stencil-based array design method such that a massive number of array design permutations can potentially exist in a microphone array stencil where $M_i \gg M_f$ and each array design can be customised for a specific frequency. Thus, if the AARM is used to generate several $f_s = 1$ -arrays with M_f -channels (such as the arrays presented in this paper) over a larger initial stencil and M_i -microphones can be purchased, then a multiplexer (also known as a MUX) can be utilised very effectively.

The initial stencil can be populated entirely with M_i -microphones that feed into a MUX. The output of the MUX can possess M_f -channels that transfer data into the typical beamforming DAQ system. The MUX can be sent switch signals, that effectively turn the necessary microphones on and off extremely quickly, such that a desired M_f -microphone array (from M_i -microphones) can be used. In other words, by sending signals to the MUX in real-time, various $f_s = 1$ -arrays can be used during experiments and can be switched between one another nearly instantaneously. For example, during an aeroacoustic test in a wind tunnel, if there are five critical beamforming frequencies to be investigated, five $f_s = 1$ -arrays can be designed using the AARM for these frequencies. Each array can be used for a specified sampling time, the microphone pressure data can be stored, a signal to the MUX is then sent to switch on the next $f_s = 1$ -array, and the process is repeated until all five arrays are tested and recorded. The implementation of a MUX here, based on the specific data presented in this paper, would lead to beamforming results comparable to arrays that far exceed the number of DAQ channels used, thus saving significant costs for smaller-scale facilities with limited budgets and also saving time, as physical plugging-and-unplugging of microphones would not be needed and the AARM is a deterministic method, meaning that no trial-and-error is required to produce each array design.

The MUX can be further utilised, to design off-centred arrays at various locations across the scanning grid, to provide better source resolution at specific regions of the scanning grid. If, for example, a large bluff body is placed in an aeroacoustic wind tunnel that possesses

two key locations of suspected noise generation, two (or more) off-centred array designs for these specific locations (regardless of f_s value) can be used to obtain a clearer understanding of the noise source generation at these specific locations. The two (or more) source maps, with localised source resolution at different locations on the scanning grid, could then be superimposed to produce a well-resolved image at both locations, thus maximising the use of the available DAQ channels. Note that each source map produced by the AARM using a MUX can be post-processed using a deconvolution technique, such as DAMAS [14] or CLEAN-SC variants [16], as each specific-frequency array has its own PSF.

The aforementioned concepts, using a MUX for different AARM $f_s = 1$ -arrays for a single source location (centred or off-centred) and/or using a MUX for different source locations, are very preliminary concepts and will be considered as future work in the recently constructed anechoic wind tunnel at The Southern University of Science and Technology, in Shenzhen, China during 2020/2021.

4 CONCLUSIONS

The AARM to date had been conducted solely on grid-based initial stencils, revealing promising performance relative to logarithmic spiral array designs with the same number of channels. In this paper, a 200-channel logarithmic spiral was used as the initial stencil and was reduced to several smaller arrays of 48-channels using multiple and single frequency source conditions, both located at and away from the scanning grid origin. The results of the AARM simulations revealed that the performance of the frequency-averaged arrays over 13 frequencies between 2 kHz and 8 kHz were degraded from the performance of the 200-channel logarithmic spiral array, as expected. Yet by using single frequency arrays, specifically for the frequency of interest, the AARM arrays using only 48-channels were comparable in MSL and MLW values to the 200-channel logarithmic spiral array for centred and off-centred conditions. While these results seemed to be a promising result, in that far fewer DAQ channels would be required to obtain the same performance as a much larger array, the practical implications of constantly changing many array designs within the stencil for different frequencies and source locations could be impractical. The concept of using a multiplexer (MUX) in conjunction with the AARM was proposed here, such that a series of single-frequency arrays can be effortlessly used in a practical environment. Provided that the initial stencil is populated with microphones, the use of each DAQ channel would be maximised and far fewer DAQ channels would be required to obtain large array beamforming results. The practical implementation of the MUX and AARM, for various single-frequency arrays, using centred and off-centred conditions, is future work.

5 ACKNOWLEDGEMENTS

This research was supported by the National Natural Science Foundation of China (Grant No. 11772146) and the Science, Technology and Innovation Commission of Shenzhen Municipality (Grant Nos. JCYJ20170817110605193 and ZDSYS201802081843517).

The primary author would also like to acknowledge Mr. Chris Morgan, a systems engineer and close friend of the primary author, who devised the idea of using a multiplexer to maximise the use of each DAQ channel and to seek optimal AARM array configurations during experiments.

References

- [1] P. Chiariotti, M. Martarelli, and P. Castellini. “Acoustic beamforming for noise source localization—reviews, methodology and applications.” *Mechanical Systems and Signal Processing*, 120, 422–448, 2019.
- [2] R. Merino-Martínez, P. Sijtsma, M. Snellen, T. Ahlefeldt, J. Antoni, C. Bahr, D. Blacodon, D. Ernst, A. Finez, S. Funke, et al. “A review of acoustic imaging methods using phased microphone arrays.” *CEAS Aeronautical Journal*, 10(1), 197–230, 2019.
- [3] R. P. Dougherty. “Spiral-shaped array for broadband imaging.” *US Patent, No. 5838284*, 1998.
- [4] Z. Prime and C. Doolan. “A comparison of popular beamforming arrays.” In *Proceedings of the Australian Acoustical Society AAS2013 Victor Harbor*, volume 1, page 5. 2013.
- [5] J. R. Underbrink. “Aeroacoustic phased array testing in low speed wind tunnels.” In *Aeroacoustic Measurements*, pages 98–217. Springer, 2002.
- [6] E. Arcondoulis, C. Doolan, L. Brooks, and A. Zander. “A modification to logarithmic spiral beamforming arrays for aeroacoustic applications.” In *Proceedings of the 17th AIAA/CEAS Aeroacoustics Conference*. AIAA Paper 2011-2720 (2011).
- [7] E. Arcondoulis, C. Doolan, A. Zander, and L. Brooks. “Design and calibration of a small aeroacoustic beamformer.” In *Proceedings of the 20th International Congress on Acoustics 2010*, volume 1, page 453. 2010.
- [8] R. P. Dougherty. “Beamforming in acoustic testing.” In *Aeroacoustic measurements*, pages 62–97. Springer, 2002.
- [9] J. Fischer and C. Doolan. “Beamforming in a reverberant environment using numerical and experimental steering vector formulations.” *Mechanical Systems and Signal Processing*, 91, 10–22, 2017.
- [10] E. Arcondoulis and Y. Liu. “Adaptive array reduction method for acoustic beamforming array designs.” *The Journal of the Acoustical Society of America*, 145(2), EL156–EL160, 2019.
- [11] E. Arcondoulis and Y. Liu. “An iterative microphone removal method for acoustic beamforming array design.” *Journal of Sound and Vibration*, 442, 552–571, 2019.
- [12] P. Sijtsma. “Optimum arrangements in a planar microphone array.” In *First CEASASC Workshop: Wind Tunnel Testing in Aeroacoustics, DNW*, volume 5, page 6. 1997.
- [13] W. Humphreys, Jr., T. Brooks, W. Hunter, Jr., and K. Meadows. “Design and use of microphone directional arrays for aeroacoustic measurements.” *36th AIAA Aerospace Sciences Meeting and Exhibit*, page 471, 1998.

- [14] T. F. Brooks and W. M. Humphreys. “A deconvolution approach for the mapping of acoustic sources (DAMAS) determined from phased microphone arrays.” *Journal of Sound and Vibration*, 294(4), 856–879, 2006.
- [15] M. Bjelić, M. Stanojević, D. Šumarac Pavlović, and M. Mijić. “Microphone array geometry optimization for traffic noise analysis.” *The Journal of the Acoustical Society of America*, 141(5), 3101–3104, 2017.
- [16] P. Sijtsma. “Clean based on spatial source coherence.” *International Journal of Aeroacoustics*, 6(4), 357–374, 2007.
- [17] E. Sarradj, A generic approach to synthesize optimal array microphone arrangements, in: *Proceedings of the 6th Berlin Beamforming Conference*, 2016, p. 4.